Bound Isoscalar Axial-Vector $bc\bar{u}\bar{d}$ Tetraquark T_{bc} from Lattice QCD Using Two-Meson and Diquark-Antidiquark Variational Basis

M. Padmanath,[1,*] Archana Radhakrishnan,[2,†] and Nilmani Mathur[2,‡]

[1]The Institute of Mathematical Sciences, a CI of Homi Bhabha National Institute, Chennai, 600113, India
[2]Department of Theoretical Physics, Tata Institute of Fundamental Research, Homi Bhabha Road, Mumbai 400005, India

(Received 11 September 2023; revised 1 April 2024; accepted 19 April 2024; published 14 May 2024)

We report a lattice QCD study of the heavy-light meson-meson interactions with an explicitly exotic flavor content $bc\bar{u}\bar{d}$, isospin $I = 0$, and axial-vector $J^P = 1^+$ quantum numbers in search of possible tetraquark bound states. The calculation is performed at four values of lattice spacing, ranging from ∼0.058 to ∼0.12 fm, and at five different values of valence light quark mass $m_{u/d}$, corresponding to pseudoscalar meson mass $M_{\rm ps}$ of about 0.5, 0.6, 0.7, 1.0, and 3.0 GeV. The energy eigenvalues in the finite volume are determined through a variational procedure applied to correlation matrices built out of two-meson interpolating operators as well as diquark-antidiquark operators. The continuum limit estimates for $D\bar{B}^*$ elastic S-wave scattering amplitude are extracted from the lowest finite-volume eigenenergies, corresponding to the ground states, using amplitude parametrizations supplemented by a lattice spacing dependence. Light quark mass $m_{u/d}$ dependence of the $D\bar{B}^*$ scattering length (a_0) suggests that at the physical pion mass $a_0^{\rm phys} = +0.57(^{+4}_{-5})(17)$ fm, which clearly points to an attractive interaction between the D and $\bar{B}^*$ mesons that is strong enough to host a real bound state T_{bc}, with a binding energy of $-43(^{+6}_{-7})(^{+14}_{-24})$ MeV with respect to the $D\bar{B}^*$ threshold. We also find that the strength of the binding decreases with increasing $m_{u/d}$ and the system becomes unbound at a critical light quark mass $m^*_{u/d}$ corresponding to $M^*_{\rm ps} = 2.73(21)(19)$ GeV.

DOI: 10.1103/PhysRevLett.132.201902

Introduction.—The discovery of a doubly charmed tetraquark [1] T_{cc} marks an important milestone [2] in spectroscopy of hadrons. Phenomenologically, doubly heavy tetraquarks in the heavy quark limit are long hypothesized to form deeply bound states [3–13] with binding energy $\mathcal{O}(100\ \text{MeV})$ with respect to the elastic strong decay threshold. While doubly bottom tetraquarks are suitable candidates for such deeply bound states, as predicted by multiple lattice QCD calculations [14–19], T_{cc} is found to be 360 keV below the lowest two-meson threshold (D^0D^{*+}). A handful of recent experimental developments involving multiple heavy quark production such as the recent discoveries of Ξ_{cc} [20], T_{cc} [2], reports of tri-J/ψ [21], associated $J/\psi\Upsilon$ [22], and di-Υ [23] productions, and recent proposals of inclusive search strategies [24,25] augment promising prospects for the doubly heavy hadron sector in the near future. In light of these advancements, a doubly heavy tetraquark with a bottom and a charm quark with a valence quark configuration $T_{bc} \equiv bc\bar{u}\bar{d}$ is going to be one of the most sought-after hadrons in this decade [26]. In this work, using lattice QCD calculations, we show a clear evidence of an attractive interaction between the D and $\bar{B}^*$ mesons that is strong enough to host a real bound state T_{bc}. This finding will further boost the search for such bottom-charm tetraquarks.

The phenomenological picture on deeply bound doubly heavy tetraquarks is based on a compact heavy diquark-light antidiquark interpretation [15,27], whereas the shallow binding energy of T_{cc} could possibly be a reflection of its dominant noncompact molecular nature [9,28]. Bottom-charm tetraquarks form an intermediate platform, where there could be complicated interplay between these pictures. A collective and refined knowledge of the low energy spectra in all these three doubly heavy systems (T_{bb}, T_{bc}, and T_{cc}) could culminate in a deeper understanding of strong interaction dynamics across a wide quark mass regime spanning from charm to bottom quarks. The isoscalar bottom-charm tetraquarks with quantum numbers $[I(J^P) = 0(1^+)]$ have been investigated previously both using lattice [29–31] and nonlattice methodologies [6,7,9,10,12,13,27,32–41]. The predictions from nonlattice approaches are quite scattered from being unbound to deeply bound, whereas the difference in conclusions from

the three existing lattice QCD investigations [29–31] call for more detailed efforts in this regard.

In this work, we perform a lattice QCD simulation of coupled $D\bar{B}^*$ and $\bar{B}D^*$ two-meson channels [42] that are the relevant lowest two strong decay thresholds, in the order of increasing energies, $E_{D\bar{B}^*} = M_{\bar{B}^*} + M_D$ and $E_{\bar{B}D^*} = M_{\bar{B}} + M_{D^*}$, where M_h is the mass of the hadron h. The extracted finite-volume ground state energies are utilized to constrain the continuum extrapolated elastic $D\bar{B}^*$ scattering amplitudes following Lüscher's finite-volume prescription [43,44]. The light quark mass $m_{u/d}$ dependence of the extracted amplitudes suggests a binding energy of $-43(^{+6}_{-7})(^{+14}_{-24})$ MeV for the $bc\bar{u}\bar{d}$ tetraquark pole with respect to $E_{D\bar{B}^*}$ at the physical point $m_{u/d}^{\text{phys}}$.

Lattice setup.—We use four lattice QCD ensembles (see Table I for relevant details) with $N_f = 2 + 1 + 1$ dynamical highly improved staggered quark (HISQ) fields generated by the MILC Collaboration [45]. The charm and strange quark masses in the sea are tuned to their respective physical values, whereas the dynamical light quark masses correspond to sea pion masses as listed in Table I. We utilize a partially quenched setup on these configurations with valence quark fields up to the charm quark masses realized using an overlap fermion action as in Refs. [46,47]. We employ a nonrelativistic QCD (NRQCD) Hamiltonian [48] for the bottom quark. Following the Fermilab prescription [49], the bare charm [50,51] and bottom [52] quark masses on each ensemble are tuned using the kinetic mass of spin averaged $1S$ quarkonia $\{a\bar{M}^{\bar{Q}Q}_{\text{kin}} = \frac{3}{4}aM_{\text{kin}}(V) + \frac{1}{4}aM_{\text{kin}}(PS)\}$ determined on the respective ensembles. The bare strange quark mass is set by equating the lattice estimate for the fictitious pseudoscalar $\bar{s}s$ meson mass to 688.5 MeV [53].

For the valence $m_{u/d}$, we investigate five different cases: three unphysical quark masses (corresponding to approximate pseudoscalar meson masses $M_{\text{ps}} \sim 0.5$, 0.6, and 1.0 GeV), the strange quark mass ($M_{\text{ps}} \sim 0.7$ GeV), and the charm quark mass ($M_{\text{ps}} \sim 3.0$ GeV). We evaluate the finite-volume spectrum for all five quark masses on all four ensembles, investigate the scattering of D and $\bar{B}^*$ mesons in all five cases and then extract the $m_{u/d}$ (otherwise M_{ps}) dependence of the scattering parameters.

TABLE I. Relevant details of the lattice QCD ensembles used. The lattice spacing estimates are measured using the r_1 parameter [45]. L_1 refers to large spatial volume, and S_1, S_2, and S_3 refer to small spatial volumes.

Label	Symbol	a [fm]	$N_s^3 \times N_t$	$M_{\text{ps}}^{\text{sea}}$
S_1	◇	0.1207(11)	$24^3 \times 64$	305
S_2	⬠	0.0888(8)	$32^3 \times 96$	312
S_3	○	0.0582(4)	$48^3 \times 144$	319
L_1	□	0.1189(9)	$40^3 \times 64$	217

Interpolators and measurements.—The finite-volume spectrum is determined from Euclidean two-point correlation functions $\mathcal{C}_{ij}(t)$, between interpolating operators $\mathcal{O}_{i,j}(\mathbf{x}, t)$ with desired quantum numbers, given by

$$\mathcal{C}_{ij}(t) = \sum_{\mathbf{x}} \left\langle \mathbb{O}_j^\dagger(0)\mathcal{O}_i(\mathbf{x}, t) \right\rangle \approx \sum_n \mathbb{Z}_j^{n\dagger} Z_i^n e^{-E^n t}. \quad (1)$$

Here E^n is the energy of the nth state and $Z_i^n = \langle 0|\mathcal{O}_i|n\rangle$ is the operator-state overlap between the sink operator $\mathcal{O}_i$ and state n. We use $\mathbb{O}$ and $\mathbb{Z}$ to represent the source operator and overlaps to distinguish them from that for the sink as we follow a wall-source to point-sink construction in our $\mathcal{C}_{ij}$ evaluations. This is a well-established procedure in ground state energy determination, despite the non-Hermitian setup in Eq. (1) (see Refs. [15,17,29,30,54,55] for details). We use the following set of linearly independent, yet Fierz related [56], operators:

$$\begin{aligned}
\mathcal{O}_1(x) &= \left[\bar{u}(x)\gamma_i b(x)\right]\left[\bar{d}(x)\gamma_5 c(x)\right] \\
&\quad - \left[\bar{d}(x)\gamma_i b(x)\right]\left[\bar{u}(x)\gamma_5 c(x)\right] \\
\mathcal{O}_2(x) &= \left[\bar{u}(x)\gamma_5 b(x)\right]\left[\bar{d}(x)\gamma_i c(x)\right] \\
&\quad - \left[\bar{d}(x)\gamma_5 b(x)\right]\left[\bar{u}(x)\gamma_i c(x)\right] \\
\mathcal{O}_3(x) &= \left[\bar{u}(x)^T\Gamma_5\bar{d}(x) - \bar{d}(x)^T\Gamma_5\bar{u}(x)\right]\left[b(x)\Gamma_i c(x)\right]. \quad (2)
\end{aligned}$$

$\mathcal{O}_1$ and $\mathcal{O}_2$ are two-meson operators of the type $D\bar{B}^*$ and $\bar{B}D^*$, respectively. $\mathcal{O}_3$ is a diquark-antidiquark type operator. Here $\Gamma_k = C\gamma_k$ with $C = i\gamma_y\gamma_t$ being the charge conjugation matrix and the diquarks (antidiquarks) in the color antitriplet (triplet) representations. Other high lying two-meson ($D^*\bar{B}^*$) and three-meson ($D\bar{B}\pi$) interpolators are ignored in this analysis as they are sufficiently high in energy to have any effects on the extracted ground states. Bilocal two-meson interpolators with nonzero internal meson momenta are also not considered, which would be an important step ahead [57]. We also compute two-point correlation functions for $\bar{B}$, $\bar{B}^*$, D, and D^* mesons, using standard local quark bilinear interpolators $(\bar{q}\Gamma Q)$ with spin structures $\Gamma \sim \gamma_5$ and γ_i for pseudoscalar and vector quantum numbers, respectively.

Analysis.—The correlation matrices $\mathcal{C}$ evaluated for the basis in Eq. (2) are analyzed following a variational procedure [58] by solving the generalized eigenvalue problem (GEVP), $\mathcal{C}(t)v^n(t) = \lambda^n(t)\mathcal{C}(t_0)v^n(t)$. The eigenvalues in the large time limit represent the time evolution the low lying eigenenergies $\mathcal{E}^n$ as $\lim_{t\to\infty}\lambda^n(t) \sim A_n e^{-\mathcal{E}^n t}$. The corresponding eigenvectors $v^n(t)$ are related to the operator-state-overlaps Z_i^n.

Eigenenergy extraction proceeds via fitting the eigenvalue correlators, $\lambda_n(t)$, or the ratios $R^n(t) = \lambda^n(t)/\mathcal{C}_{m_1}(t)\mathcal{C}_{m_2}(t)$, with the expected asymptotic exponential behavior. Here, $\mathcal{C}_{m_i}$ is the two-point correlation function for the meson m_i. $R^n(t)$ is empirically known to efficiently

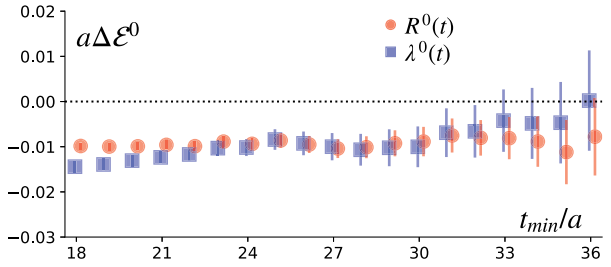

FIG. 1. $t_{\rm min}$ dependence of the $\Delta\mathcal{E}^0$ fit estimates determined from the fits to λ^0 and $R^0(t)$ for the case $M_{\rm ps} \sim 700$ MeV in the finest ensemble. Here the superscript 0 refers to the lowest eigenenergy.

mitigate correlated noise between the product of two single hadron correlators and the interacting correlator for the two-hadron system [59]. Note that the automatic cancellation of the additive quark mass offset, inherent to NRQCD formulation, is an added advantage in using $R^n(t)$ for the fits. The systematics associated with the chosen time interval for fitting are assessed by varying the lower boundary of the time interval, $t_{\rm min}$, with a fixed upper boundary, $t_{\rm max}$, chosen considering the noise level. In Fig. 1, we present a representative plot showing this $t_{\rm min}$ dependence of the energy splittings ($\Delta\mathcal{E}^n$) determined from the fits to $\lambda^n(t)$ and $R^n(t)$, respectively. The energy differences are evaluated from $\lambda^n(t)$ using the relation $\Delta\mathcal{E}^n = \mathcal{E}^n - M_{m_1} - M_{m_2}$, whereas the fits to $R^n(t)$ directly yield the respective estimates. We choose the optimal $t_{\rm min}$ values where the two different procedures are found to agree asymptotically in time. We also perform additional checks considering an alternative quark smearing with different smearing widths to affirm our energy estimates; see Appendix A. Our final results are based on fitting the ratio correlators $R^n(t)$.

Finite-volume eigenenergies.—In Fig. 2, we present the finite-volume GEVP eigenenergies, in lattice units, for the isoscalar axial-vector $bc\bar{u}\bar{d}$ channel. The results shown are for the L_1 ensemble at the five different $m_{u/d}$ values corresponding to $M_{\rm ps} \sim 0.5$, 0.6, 0.7, 1.0, and 3.0 GeV. Note that these estimates include the additive offsets related

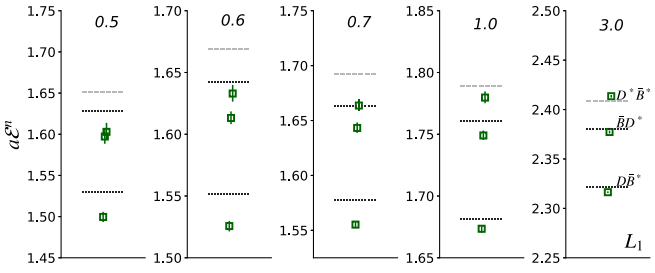

FIG. 2. The GEVP eigenenergies in finite-volume for isoscalar axialvector $bc\bar{u}\bar{d}$ channel on the L_1 ensemble. Five panels show the results obtained at various pseudoscalar meson masses ($M_{\rm ps}$) 0.5, 0.6, 0.7, 1.0, and 3.0, respectively.

to the NRQCD-based bottom quark dynamics. The noninteracting two-meson energy levels corresponding to $D\bar{B}^*$ and $\bar{B}D^*$ thresholds are indicated as dotted horizontal line segments and those related to $\bar{B}^*D^*$ threshold by dashed lines for each $M_{\rm ps}$. The lowest eigenenergy or the ground state energy is dominated by the Z_1^0 factor corresponding to $\mathcal{O}_1$, that is related to the $D\bar{B}^*$ threshold and is determined unambiguously by the operator $\mathcal{O}_1$; see Ref. [60] for details. The most important observation is a clear trend for negative energy shifts in the ground state energies, which can be observed in all the cases, indicating a possible attractive interaction between the D and $\bar{B}^*$ mesons [63]. A similar pattern of low lying eigenenergies and ground state negative energy shifts are also observed in other ensembles; see details in Ref. [60]. We expect that for our choice of interpolating operators and the accessible values of t, $\mathcal{E}^0$ will be an accurate estimate of E^0, whereas our setup is unable to accurately estimate excited-state energies. This means the excited eigenenergies presented in Fig. 2 may not correspond to the higher lying elastic excitations of the $D\bar{B}^*$ channel. The location of the lowest two noninteracting finite-volume levels related to the $D\bar{B}^*$ channel along with the ground state eigenenergies are presented in Appendix B. Hence we focus only on the ground state energies ($\mathcal{E}^0 \sim E^0$) for the rest of the analysis.

In Fig. 3, we present the ground state energy estimates, in units of $E_{D\bar{B}^*}$, at various $M_{\rm ps}$ and for all the ensembles. These estimates are evaluated as $E^n = \Delta E^n + M_D + \tilde{M}_{\bar{B}^*}$, where ΔE^n is the estimate from fit to $R^n(t)$, $\tilde{M}_{\bar{B}^*} = M_{\bar{B}^*} - 0.5\bar{M}^{\bar{b}b}_{\rm lat} + 0.5\bar{M}^{\bar{b}b}_{\rm phys}$ accounts for the NRQCD additive offset, and $\bar{M}^{\bar{b}b}_{\rm lat}(\bar{M}^{\bar{b}b}_{\rm phys})$ refers to the spin averaged mass of the $1S$ bottomonium measured on the lattice (experiments). The eigenenergies clearly show a trend of decreasing energy spitting, hence decreasing interaction strength, with increasing $M_{\rm ps}$. Another interesting feature to note here is the nonzero lattice spacing (a) dependence of the ground state energies on similar volume ensembles (S_1, S_2, S_3), which we account for through an a dependence in the parametrized amplitude as discussed below.

In Fig. 3, we also indicate the branch point location of the left-hand cut (lhc) arising out of an off-shell pion exchange process for different $M_{\rm ps}$ by horizontal dashed lines. Recent developments point to the importance of lhc effects on virtual subthreshold poles related to the T_{cc} tetraquark [64]. Such effects on bound states are the subject of future studies where one could successfully solve the relevant three particle integral equations. This is beyond the scope of this work and we ignore such effects in our analysis.

$D\bar{B}^*$ scattering amplitude.—Assuming these energy splittings in ground states are purely described by elastic scattering in the $D\bar{B}^*$ system, we utilize them to constrain the associated S-wave scattering amplitude following

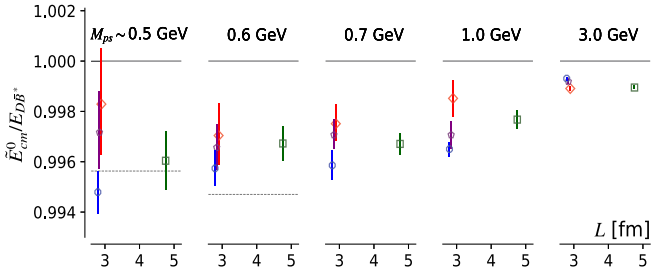

FIG. 3. The ground state energies in units of $E_{D\bar{B}^*}$ on all ensembles (see Table I for color-symbol conventions) for all $M_{\rm ps}$ values (different vertical panels).

Lüscher's finite-volume prescription [43,44]. For the low energy scattering of D and $\bar{B}^*$ mesons, where other multiparticle thresholds are sufficiently high [65], in the S-wave leading to the total angular momentum and parity $J^P = 1^+$, the scattering phase shifts $\delta_{l=0}(k)$ are related to the finite-volume energy spectrum through $kcot[\delta_0(k)] = 2Z_{00}[1;(kL/2\pi)^2)]/(L\sqrt{\pi})$. Here, $k(E_{cm} = \sqrt{s})$ is the momentum (energy) in the center-of-momentum frame such that $4sk^2 = (s-(M_D+M_{\bar{B}^*})^2)(s-(M_D-M_{\bar{B}^*})^2)$. We follow the procedure outlined in Appendix B of Ref. [66] to constrain the amplitude. A subthreshold pole in the S-wave scattering amplitude $t = (\cot\delta_0 - i)^{-1}$ occurs when $k\cot\delta_0 = \pm\sqrt{-k^2}$ for scattering in the S-wave.

We parametrize the elastic $D\bar{B}^*$ scattering amplitude in terms of the scattering length a_0 in an effective range expansion near the threshold, supplemented by a lattice spacing dependence. This is required to incorporate the cutoff effects observed in the ground state energy estimates. We find that a linear functional form given by $k\cot\delta_0 = A^{[0]} + aA^{[1]}$, where $A^{[0]} = -1/a_0$, accommodates the a dependence of the $k\cot\delta_0$ estimates. We present the fit results for $A^{[0]} = -1/a_0$ in Fig. 4 (circle symbols) as a function of $M_{\rm ps}$ involved. Alternative fitting choices with a leading quadratic dependence or using only data from

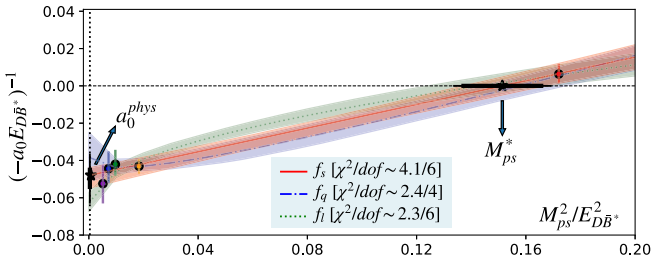

FIG. 4. Continuum extrapolated $k\cot\delta_0$ or $A^{[0]} = -1/a_0$ estimates of the $D\bar{B}^*$ system as a function of $M^2_{\rm ps}$ in units of $E_{D\bar{B}^*}$. The dotted vertical line close to the y axis indicates $M_{\rm ps} = M_\pi^{\rm phys}$. The two star symbols represent the amplitude at $M_{\rm ps} = M_\pi^{\rm phys}$ and the critical $M_{\rm ps} = M^*_{\rm ps}$ above which the system becomes unbound.

noncharm $M_{\rm ps}$ are consistent with results in Fig. 4; see details in Supplemental Material [60].

The sign of $A^{[0]} = -1/a_0$ determines the fate of the near-threshold pole, if there exists one. A negative (positive) value of $A^{[0]}(a_0)$ indicates that the interaction potential is strong enough to form a real bound state [67]. After considering all possible systematics, we find that for all the noncharm light quark masses, $A^{[0]}$ is negative, which indicates an attractive interaction strong enough to host a real bound state. On the contrary, at the charm point, despite the unambiguous negative energy shifts in the ground states, the attraction is weak to host any real bound state as suggested by the positive value of $k\cot\delta_0$ in the continuum limit. This observation goes in line with the phenomenological expectation for doubly heavy four quark ($QQ'l_1l_2$) systems with $m_{l_1} = m_{l_2}$ that the binding increases with increased relative heaviness of the heavy quarks with respect to its light quark content [15,27,68].

Now we investigate the light quark mass ($m_{u/d}$) or $M_{\rm ps}$ dependence of the fitted parameters. To this end, we consider three different parametrizations: a linear dependence $[f_l(M_{\rm ps}) = \alpha_c + \alpha_l M_{\rm ps}]$ to probe the heavy light quark mass case, a leading $M^2_{\rm ps}$ dependence $[f_s(M_{\rm ps}) = \beta_c + \beta_s M^2_{\rm ps}]$ to assess the chiral behavior, and a quadratic dependence $[f_q(M_{\rm ps}) = \theta_c + \theta_l M_{\rm ps} + \theta_s M^2_{\rm ps}]$ to quantify the associated systematics. In Fig. 4, we show the fit results for this $M_{\rm ps}$ dependence in colored bands. The two stars represent $A^{[0]}$ at the physical $M_{\rm ps}$ (equivalently the physical scattering length $a_0^{\rm phys}$) and the critical $M_{\rm ps}$ at which $A^{[0]}$ changes its sign or above which the system becomes unbound. It is indeed desired to have more points in the intermediate mass regime between the charm and the strange quark masses to further constrain the dependence. Yet, our fits demonstrate near independence in the fit forms as can be observed from the consistency between the error bands from different fit forms.

Based on the fit form $f_s(M_{\rm ps})$ in the chiral regime, we find that the scattering length of the $D\bar{B}^*$ system at the physical light quark mass ($m^{\rm phys}_{u/d}$), corresponding to $M_{\rm ps} = M_\pi^{\rm phys}$, to be

$$a_0^{\rm phys} = 0.57(^{+4}_{-5})(17)\ \text{fm}. \tag{3}$$

The asymmetric errors indicate the statistical uncertainties, whereas the second parenthesis quotes the systematic uncertainties with the most dominant contribution arising from the chiral extrapolation fit forms. The positive value of the scattering length at $M_{\rm ps} = M_\pi^{\rm phys}$, at the level of 3σ uncertainty, is an unambiguous evidence for the strength of the $D\bar{B}^*$ interaction potential to host a real $bc\bar{u}\bar{d}$ tetraquark bound state T_{bc} with binding energy

$$\delta m_{T_{bc}} = -43(^{+6}_{-7})(^{+14}_{-24})\ \text{MeV}, \tag{4}$$

with respect to $E_{D\bar{B}^*}$. The first parenthesis indicates the statistical errors and the second one quantifies various systematic uncertainties added in quadrature. The pseudoscalar meson mass, corresponding to the critical light quark mass, where a_0 diverges, is found to be $M^*_{\rm ps} = 2.73(21)(19)$ GeV. This critical point also signifies that QCD dynamics within such exotic systems is such that at a heavy light quark mass the system of quarks perhaps reaches the unitary gas limit, as indicated by the divergent scattering length [69]. For $M_{\rm ps} \geq M^*_{\rm ps}$, the T_{bc} system remains unbound.

Systematic uncertainties.—Our lattice setup together with the bare bottom and charm quark mass tuning procedure has been demonstrated to reproduce the $1S$ hyperfine splittings in quarkonia with uncertainties less than 6 MeV [52,55]. We observe the effects of such a mistuning of either of the heavy quark mass on the energy splittings we extract are very small compared to the statistical errors. Additionally, our strategy of evaluating the energy differences and working with mass ratios has also been shown to significantly mitigate the systematic uncertainties related to heavy quark masses [54,55]. This is observed to be the case in this study as well, leading to transparent signals for the ground state energy as shown in Figs. 1, 2, and 3. Our fitting procedure involves careful and conservative determination of statistical errors, and uncertainties related to the excited-state-contamination and fit-window errors. Additional checks using alternative quark smearing procedures also agree with our energy estimates, see Appendix A. The amplitude determination and followed extrapolations are performed with results from varying the fit windows to evaluate the uncertainties propagated to our final results. The uncertainties related to the fit forms used in chiral extrapolations are observed to be the most dominant, as is evident from Fig. 4. We assume the partially quenched setup involving ensembles with different sea pion masses, we utilize, have negligible effects on the energy splittings we extract for the explicitly exotic T_{bc} tetraquark, similar to what was observed for heavy hadrons in Refs. [70,71]. Uncertainty related to scale setting is also found to be negligible in comparison to the statistical uncertainties in the energy splittings.

Summary.—We have performed a lattice QCD simulation of coupled $D\bar{B}^* - \bar{B}D^*$ scattering with explicitly exotic flavor $bc\bar{u}\bar{d}$ and $I(J^P) = 0(1^+)$. Following a rigorous extraction of finite-volume eigenenergies and continuum extrapolated elastic $D\bar{B}^*$ scattering amplitudes for the five light quark masses studied, we determine the light quark mass dependence of the elastic $D\bar{B}^*$ scattering length a_0. We observe unambiguous negative energy shifts between the interacting and noninteracting finite-volume energy levels. Our estimate for $a_0^{\rm phys}$ [Eq. (3)] is positive, indicating an attractive interaction between the D and $\bar{B}^*$ mesons, which is strong enough to host a real bound state with binding energy $\delta m_{T_{bc}} = -43(^{+6}_{-7})(^{+14}_{-24})$ MeV. We find that the strength of interaction is such that this $bc\bar{u}\bar{d}$ tetraquark becomes unbound at $M^*_{\rm ps}$, which is close to the η_c meson mass.

In this work, we make several important steps ahead to arrive at robust inference on the nature of interaction between the D and $\bar{B}^*$ mesons. Our main strategy has been to determine the signature of scattering length in $D\bar{B}^*$ interactions at the physical pion mass $a_0^{\rm phys}$. Our results indicate that $a_0^{\rm phys}$ is positive, which suggests that attractive $D\bar{B}^*$ interactions are strong enough to host a real bound state. Further theoretical investigations are desired to reduce the uncertainties in the binding energy of T_{bc} with respect to $E_{D\bar{B}^*}$. Fully dynamical simulations on several more ensembles, with different volumes and improvised fermion actions, high statistics studies with lighter $m_{u/d}$, etc. are a few other improvisations that can further constrain the relevant scattering amplitude. Additionally, future works involving Hermitian correlation matrices at rest as well as in moving frames and those using bilocal two-meson interpolators with nonzero relative meson momenta aimed at reliable excited state extraction would be a few important steps ahead [57,66,72,73]. We hope that our observations and inferences in this work will motivate more theoretical efforts and experimental searches for such states.

This work is supported by the Department of Atomic Energy, Government of India, under Project Identification Number RTI 4002. M. P. gratefully acknowledges support from the Department of Science and Technology, India, SERB Start-up Research Grant No. SRG/2023/001235. We are thankful to the MILC Collaboration and in particular to S. Gottlieb for providing us with the HISQ lattice ensembles. We thank Sara Collins for a careful reading of the manuscript. We thank the authors of Ref. [74] for making the *TwoHadronsInBox* package utilized in this work. We also thank Gunnar Bali, Parikshit Junnarkar, Alexey Nefediev, Sayantan Sharma, Stephen R. Sharpe, and Tanishk Shrimal for discussions. Computations were carried out on the Cray-XC30 of ILGTI, TIFR. Amplitude analyses were performed on Nandadevi computing cluster at IMSc Chennai. N. M. would also like to thank A. Salve and K. Ghadiali for computational support.

Appendix A: Ground state energy plateau.—In this work we have utilized a wall-source point-sink setup to construct the necessary two-point correlation functions. The use of such an asymmetric setup implies the effective energies $aE_{\rm eff} = [\ln(C(t)/C(t+\delta t))]/\delta t$ could approach their asymptotic values as rising-from-below, due to the nonpositive definite nature of the coefficients in a spectral decomposition, in contrast to a

falling-from-above behavior in a symmetric setup. In Fig. 5, we show the effective mass in wall-source point-sink setup with the brown circle ($R^2 = 0$) which rises from below.

To avoid any ambiguity in selecting the plateau regions of effective masses of such correlators, we also employ a wall-source box-sink setup [30], which asymptotically approaches the symmetric limit. In the symmetric limit, the effective masses are expected to follow a conventional falling-from-above feature, modulo the statistical noise. To this end, we vary the smearing radius R to investigate the time dependence of effective mass plateaus in the approach to the symmetric limit. In Fig. 5, we present a comparison of the effective energy (top) and effective energy splittings (bottom) determined using different quark sink smearing procedures for the case of $M_{\rm ps} \sim 700$ MeV on the finest ensemble. Clearly the rising-from-below behavior is gradually disappearing in the approach to the symmetric limit. It is also evident that the results at the large time limit from point-sink and box-sink are very much consistent with each other affirming our assessment on effective mass plateau in choosing a fit range. Such a behavior of effective masses with varying smearing radii was also observed in Ref. [30]. In the large time limit, where the signal quality is still good, all of sink smearing cases suggest consistent negative energy shifts. This is evident from the large time behavior of energy splittings presented in the bottom panel of Fig. 5, where the correlated statistical noise, not related to the excited state contamination, is suppressed between the numerator and denominator in the ratio correlators $R^n(t)$.

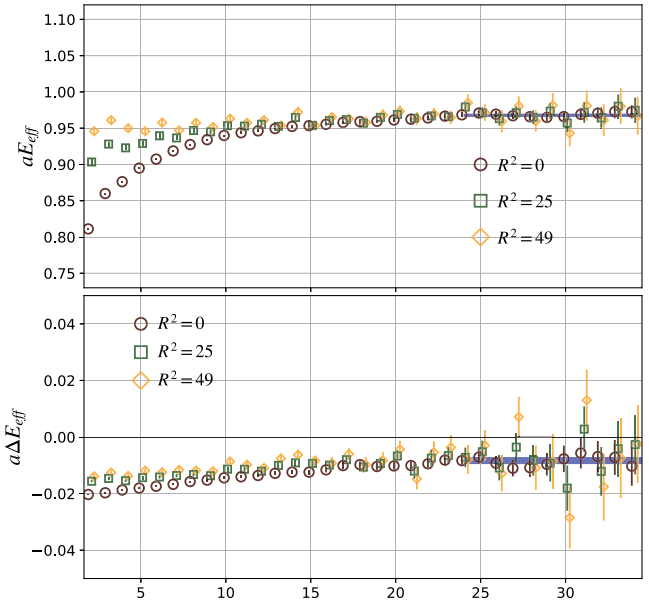

FIG. 5. Comparison of effective energy (top) and effective energy splitting (bottom) for the ground state as determined using three different smearing radii applied on the quark fields at the sink timeslice. The legend indicates the smearing radius squared in units of the lattice spacing [30]. The blue horizontal band indicates the final fit estimate for the energy and energy splitting. The results presented are for the case $M_{\rm ps} \sim 700$ MeV on the finest ensemble.

The agreement of energy splitting estimates from fits to $R^n(t)$ with those evaluated from separate fits to the GEVP eigenvalue correlators $\lambda^n(t)$ and the single-meson correlators $\mathcal{C}_{D/\bar{B}^*}$ at large times (see Fig. 1) already rules out the usual concern of accidental partial cancellation of excited state contaminations in $R^n(t)$. The consistency at large times between ground state energy plateaus from different sink-smearing radii observed in top panel of Fig. 5 further affirms the reliable isolation of the ground state plateau. Note also that the magnitude of such cancellations and the ground state saturation times could be different in different lattice QCD ensembles. All the ground state estimates for noncharm $M_{\rm ps}$ values in our study are determined from the time intervals approximately between 1.5(2) fm [$t_{\rm min}$] to 2.3(2) fm [$t_{\rm max}$]. The consistent ground state saturation times across different ensembles with different specifications further imply the reliability of our ground state saturation, despite our asymmetric setup.

Appendix B: Elastic $D\bar{B}^*$ excitations.—Gaining access to higher lying elastic excitations in the $D\bar{B}^*$ channel is an important step ahead toward constraining the energy dependence of the amplitude over a long energy range. However, within the wall-smearing setup, all the nonzero momentum excitations are significantly suppressed. This suppression is exact in a free theory, and is empirically confirmed from the early plateauing and from the quality of signals in the interacting theory. While this suppression is advantageous in ground state energy determination (see Refs. [15,17,29,30,54,55] for details), the suppressed coupling to the nonzero momentum excitations implies that the access to higher two-meson elastic excitations with nonzero relative meson momenta are restricted in the wall-smearing setup. This implies other methodologies that facilitate the use of bilocal two-meson interpolators with separately momentum projected mesons are necessary in future studies [57,75,76]. (Recently, Ref. [77] appeared which utilizes bilocal two-meson interpolators in their analysis, utilizing the methods in Ref. [75].) In this respect, it is informative to know the location of the lowest noninteracting level with nonzero relative meson momenta and whether it is close enough to influence the ground state energies in any substantial way. Considering this, in Fig. 6 we present the ground state eigenenergies along with the $D\bar{B}^*$ threshold and the next lowest elastic $D\bar{B}^*$ excitation with nonzero relative meson momentum determined using the continuum dispersion relation that is assumed in the finite-volume

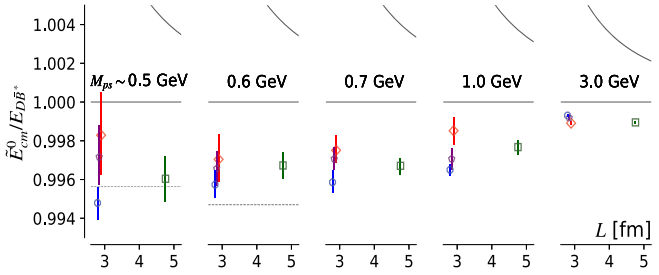

FIG. 6. The ground state energy eigenvalues in the background of lowest two noninteracting $D\bar{B}^*$ finite-volume levels in units of $E_{D\bar{B}^*}$ on all ensembles (see Table I for symbol conventions) for all $M_{\rm ps}$ values (different vertical panels).

quantization condition [43,44]. Clearly, the location of this first noninteracting elastic excitation is sufficiently high to have any non-negligible effects on the extracted the ground state energies.

*padmanath@imsc.res.in
†archana.radhakrishnan@tifr.res.in
‡nilmani@theory.tifr.res.in

[1] We follow the nomenclature that a "tetraquark" refers to any bound state or resonance with dominant four-quark Fock component, whether it is a compact four-quark object or a two-meson molecule or a mixture of both.
[2] R. Aaij *et al.* (LHCb Collaboration), Observation of an exotic narrow doubly charmed tetraquark, Nat. Phys. **18**, 751 (2022).
[3] J. P. Ader, J. M. Richard, and P. Taxil, Do narrow heavy multiquark states exist?, Phys. Rev. D **25**, 2370 (1982).
[4] J. l. Ballot and J. M. Richard, Four quark states in additive potentials, Phys. Lett. **123B**, 449 (1983).
[5] S. Zouzou, B. Silvestre-Brac, C. Gignoux, and J. M. Richard, Four quark bound states, Z. Phys. C **30**, 457 (1986).
[6] L. Heller and J. A. Tjon, On the existence of stable dimesons, Phys. Rev. D **35**, 969 (1987).
[7] J. Carlson, L. Heller, and J. A. Tjon, Stability of dimesons, Phys. Rev. D **37**, 744 (1988).
[8] A. V. Manohar and M. B. Wise, Exotic QQqq states in QCD, Nucl. Phys. **B399**, 17 (1993).
[9] D. Janc and M. Rosina, The $T_{cc} = DD^*$ molecular state, Few-Body Syst. **35**, 175 (2004).
[10] D. Ebert, R. N. Faustov, V. O. Galkin, and W. Lucha, Masses of tetraquarks with two heavy quarks in the relativistic quark model, Phys. Rev. D **76**, 114015 (2007).
[11] F. S. Navarra, M. Nielsen, and S. H. Lee, QCD sum rules study of $QQ - \bar{u}\bar{d}$ mesons, Phys. Lett. B **649**, 166 (2007).
[12] E. J. Eichten and C. Quigg, Heavy-quark symmetry implies stable heavy tetraquark mesons $Q_iQ_j\bar{q}_k\bar{q}_l$, Phys. Rev. Lett. **119**, 202002 (2017).
[13] M. Karliner and J. L. Rosner, Discovery of doubly charmed Ξ_{cc} baryon implies a stable $(bb\bar{u}\bar{d})$ tetraquark, Phys. Rev. Lett. **119**, 202001 (2017).
[14] P. Bicudo, K. Cichy, A. Peters, and M. Wagner, *BB* interactions with static bottom quarks from Lattice QCD, Phys. Rev. D **93**, 034501 (2016).
[15] A. Francis, R. J. Hudspith, R. Lewis, and K. Maltman, Lattice prediction for deeply bound doubly heavy tetraquarks, Phys. Rev. Lett. **118**, 142001 (2017).
[16] P. Bicudo, M. Cardoso, A. Peters, M. Pflaumer, and M. Wagner, $ud\bar{b}\bar{b}$ tetraquark resonances with lattice QCD potentials and the Born-Oppenheimer approximation, Phys. Rev. D **96**, 054510 (2017).
[17] P. Junnarkar, N. Mathur, and M. Padmanath, Study of doubly heavy tetraquarks in lattice QCD, Phys. Rev. D **99**, 034507 (2019).
[18] L. Leskovec, S. Meinel, M. Pflaumer, and M. Wagner, Lattice QCD investigation of a doubly bottom $\bar{b}\bar{b}ud$ tetraquark with quantum numbers $I(J^P) = 0(1^+)$, Phys. Rev. D **100**, 014503 (2019).
[19] R. J. Hudspith and D. Mohler, Exotic tetraquark states with two $\bar{b}$ quarks and $J^P = 0^+$ and 1^+B_s states in a non-perturbatively tuned lattice NRQCD setup, Phys. Rev. D **107**, 114510 (2023).
[20] R. Aaij *et al.* (LHCb Collaboration), Observation of the doubly charmed baryon Ξ_{cc}^{++}, Phys. Rev. Lett. **119**, 112001 (2017).
[21] A. Tumasyan *et al.* (CMS Collaboration), Observation of triple J/ψ meson production in proton-proton collisions, Nat. Phys. **19**, 338 (2023); **19**, 461(E) (2023).
[22] R. Aaij *et al.* (LHCb Collaboration), Associated production of prompt J/ψ and Υ mesons in pp collisions at $\sqrt{s} = 13$ TeV, J. High Energy Phys. 08 (2023) 093.
[23] V. Khachatryan *et al.* (CMS Collaboration), Observation of $\Upsilon(1S)$ pair production in proton-proton collisions at $\sqrt{s} = 8$ TeV, J. High Energy Phys. 05 (2017) 013.
[24] T. Gershon and A. Poluektov, Displaced B_c^- mesons as an inclusive signature of weakly decaying double beauty hadrons, J. High Energy Phys. 01 (2019) 019.
[25] Q. Qin, Y.-J. Shi, W. Wang, G.-H. Yang, F.-S. Yu, and R. Zhu, Inclusive approach to hunt for the beauty-charmed baryons Ξ_{bc}, Phys. Rev. D **105**, L031902 (2022).
[26] I. Polyakov, Doubly charmed tetraquarks T_{cc} and new road it opens, in *Proceedings of the 20th International Conference on Hadron Spectroscopy and Structure* (2023), https://agenda.infn.it/event/33110/contributions/201598/attachments/106521/150070/Hadron2023_Polyakov.pdf.
[27] A. Czarnecki, B. Leng, and M. B. Voloshin, Stability of tetrons, Phys. Lett. B **778**, 233 (2018).
[28] S. S. Agaev, K. Azizi, and H. Sundu, Hadronic molecule model for the doubly charmed state T_{cc}^+, J. High Energy Phys. 06 (2022) 057.
[29] A. Francis, R. J. Hudspith, R. Lewis, and K. Maltman, Evidence for charm-bottom tetraquarks and the mass dependence of heavy-light tetraquark states from lattice QCD, Phys. Rev. D **99**, 054505 (2019).
[30] R. J. Hudspith, B. Colquhoun, A. Francis, R. Lewis, and K. Maltman, A lattice investigation of exotic tetraquark channels, Phys. Rev. D **102**, 114506 (2020).
[31] S. Meinel, M. Pflaumer, and M. Wagner, Search for $\bar{b}\bar{b}us$ and $\bar{b}\bar{c}ud$ tetraquark bound states using lattice QCD, Phys. Rev. D **106**, 034507 (2022).
[32] W. Chen, T. G. Steele, and S.-L. Zhu, Exotic open-flavor $bc\bar{q}\bar{q}$, $bc\bar{s}\bar{s}$ and $qc\bar{q}\bar{b}$, $sc\bar{s}\bar{b}$ tetraquark states, Phys. Rev. D **89**, 054037 (2014).

[33] S. Sakai, L. Roca, and E. Oset, Charm-beauty meson bound states from $B(B^*)D(D^*)$ and $B(B^*)\bar{D}(\bar{D}^*)$ interaction, Phys. Rev. D **96**, 054023 (2017).

[34] T. F. Caramés, J. Vijande, and A. Valcarce, Exotic $bc\bar{q}\bar{q}$ four-quark states, Phys. Rev. D **99**, 014006 (2019).

[35] W. Park, S. Noh, and S. H. Lee, Masses of the doubly heavy tetraquarks in a constituent quark model, Nucl. Phys. A **A983**, 1 (2019).

[36] C. Deng, H. Chen, and J. Ping, Systematical investigation on the stability of doubly heavy tetraquark states, Eur. Phys. J. A **56**, 9 (2020).

[37] G. Yang, J. Ping, and J. Segovia, Doubly-heavy tetraquarks, Phys. Rev. D **101**, 014001 (2020).

[38] S. S. Agaev, K. Azizi, and H. Sundu, Double-heavy axial-vector tetraquark $T^0_{bc;\bar{u}\bar{d}}$, Nucl. Phys. **B951**, 114890 (2020).

[39] Q.-F. Lü, D.-Y. Chen, and Y.-B. Dong, Masses of doubly heavy tetraquarks $T_{QQ'}$ in a relativized quark model, Phys. Rev. D **102**, 034012 (2020).

[40] Y. Tan, W. Lu, and J. Ping, Systematics of $QQ\bar{q}\bar{q}$ in a chiral constituent quark model, Eur. Phys. J. Plus **135**, 716 (2020).

[41] E. Braaten, L.-P. He, and A. Mohapatra, Masses of doubly heavy tetraquarks with error bars, Phys. Rev. D **103**, 016001 (2021).

[42] We work in the isosymmetric limit with no QED effects and $m_u = m_d$. Hence we choose to call the degenerate $(D^+B^-, D^0\bar{B}^0)$ threshold as $D\bar{B}$, and equivalently for others like $D\bar{B}^*$, $\bar{B}D^*$ and $D^*\bar{B}^*$.

[43] M. Luscher, Two-particle states on a torus and their relation to the scattering matrix, Nucl. Phys. **B354**, 531 (1991).

[44] R. A. Briceno, Two-particle multichannel systems in a finite volume with arbitrary spin, Phys. Rev. D **89**, 074507 (2014).

[45] A. Bazavov *et al.* (MILC Collaboration), Lattice QCD ensembles with four flavors of highly improved staggered quarks, Phys. Rev. D **87**, 054505 (2013).

[46] Y. Chen, S. J. Dong, T. Draper, I. Horvath, F. X. Lee, K. F. Liu, N. Mathur, and J. B. Zhang, Chiral logarithms in quenched QCD, Phys. Rev. D **70**, 034502 (2004).

[47] A. Li *et al.* (xQCD Collaboration), Overlap valence on $2+1$ flavor domain wall fermion configurations with deflation and low-mode substitution, Phys. Rev. D **82**, 114501 (2010).

[48] G. P. Lepage, L. Magnea, C. Nakhleh, U. Magnea, and K. Hornbostel, Improved nonrelativistic QCD for heavy quark physics, Phys. Rev. D **46**, 4052 (1992).

[49] A. X. El-Khadra, A. S. Kronfeld, and P. B. Mackenzie, Massive fermions in lattice gauge theory, Phys. Rev. D **55**, 3933 (1997).

[50] S. Basak, S. Datta, M. Padmanath, P. Majumdar, and N. Mathur, Charm and strange hadron spectra from overlap fermions on HISQ gauge configurations, Proc. Sci. LATTICE2012 (**2012**) 141.

[51] S. Basak, S. Datta, A. T. Lytle, M. Padmanath, P. Majumdar, and N. Mathur, Hadron spectra from overlap fermions on HISQ gauge configurations, Proc. Sci. LATTICE2013 (**2014**) 243.

[52] N. Mathur, M. Padmanath, and R. Lewis, Charmed-bottom mesons from lattice QCD, Proc. Sci. LATTICE2016 (**2016**) 100.

[53] B. Chakraborty, C. T. H. Davies, B. Galloway, P. Knecht, J. Koponen, G. C. Donald, R. J. Dowdall, G. P. Lepage, and C. McNeile, High-precision quark masses and QCD coupling from $n_f = 4$ lattice QCD, Phys. Rev. D **91**, 054508 (2015).

[54] N. Mathur, M. Padmanath, and S. Mondal, Precise predictions of charmed-bottom hadrons from lattice QCD, Phys. Rev. Lett. **121**, 202002 (2018).

[55] N. Mathur, M. Padmanath, and D. Chakraborty, Strongly bound dibaryon with maximal beauty flavor from lattice QCD, Phys. Rev. Lett. **130**, 111901 (2023).

[56] M. Padmanath, C. B. Lang, and S. Prelovsek, X(3872) and Y(4140) using diquark-antidiquark operators with lattice QCD, Phys. Rev. D **92**, 034501 (2015).

[57] M. Wagner, C. Alexandrou, J. Finkenrath, T. Leontiou, S. Meinel, and M. Pflaumer, Lattice QCD study of antiheavy-antiheavy-light-light tetraquarks based on correlation functions with scattering interpolating operators both at the source and at the sink, Proc. Sci. LATTICE2022 (**2023**) 270.

[58] C. Michael, Adjoint sources in lattice gauge theory, Nucl. Phys. **B259**, 58 (1985).

[59] J. R. Green, A. D. Hanlon, P. M. Junnarkar, and H. Wittig, Weakly bound H dibaryon from SU(3)-flavor-symmetric QCD, Phys. Rev. Lett. **127**, 242003 (2021).

[60] See Supplemental Material, which includes Refs. [56,61,62], at http://link.aps.org/supplemental/10.1103/PhysRevLett.132.201902 for various technical details of the work: Finite-volume eigeneneergies on all lattice QCD ensembles, amplitude fits, and quark mass dependence fits are shown here.

[61] J. J. Dudek, R. G. Edwards, M. J. Peardon, D. G. Richards, and C. E. Thomas, Highly excited and exotic meson spectrum from dynamical lattice QCD, Phys. Rev. Lett. **103**, 262001 (2009).

[62] M. Padmanath, R. G. Edwards, N. Mathur, and M. Peardon, Spectroscopy of triply charmed baryons from lattice QCD, Phys. Rev. D **90**, 074504 (2014).

[63] We also observe statistically significant negative energy shifts of similar magnitude for the ground states in $D\bar{B}$ two-meson energy spectrum at different light quark masses with isoscalar scalar $[I(J^P) = 0(0^+)]$ quantum numbers and explicitly exotic flavor content $bc\bar{u}\bar{d}$. This work is reported in Ref. [78].

[64] M.-L. Du, A. Filin, V. Baru, X.-K. Dong, E. Epelbaum, F.-K. Guo, C. Hanhart, A. Nefediev, J. Nieves, and Q. Wang, Role of left-hand cut contributions on pole extractions from lattice data: Case study for $T_{cc}(3875)^+$, Phys. Rev. Lett. **131**, 131903 (2023).

[65] Z. T. Draper and S. R. Sharpe, Applicability of the two-particle quantization condition to partially-quenched theories, Phys. Rev. D **104**, 034510 (2021).

[66] M. Padmanath and S. Prelovsek, Signature of a doubly charm tetraquark pole in DD^* scattering on the lattice, Phys. Rev. Lett. **129**, 032002 (2022).

[67] L. D. Landau and E. M. Lifshitz, *Quantum Mechanics: Non-Relativistic Theory*, Course of Theoretical Physics Vol. v.3 (Butterworth-Heinemann, Oxford, 1991).

[68] P. Junnarkar, M. Padmanath, and N. Mathur, Heavy light tetraquarks from lattice QCD, EPJ Web Conf. **175**, 05014 (2018).

[69] R. G. Newton, *Scattering Theory of Waves and Particles* (Springer, Berlin, Heidelberg, 2013), 10.1007/978-3-642-88128-2.

[70] R. J. Dowdall, C. T. H. Davies, T. C. Hammant, and R. R. Horgan, Precise heavy-light meson masses and hyperfine splittings from lattice QCD including charm quarks in the sea, Phys. Rev. D **86**, 094510 (2012).

[71] C. McNeile, C. T. H. Davies, E. Follana, K. Hornbostel, and G. P. Lepage, Heavy meson masses and decay constants from relativistic heavy quarks in full lattice QCD, Phys. Rev. D **86**, 074503 (2012).

[72] M. Padmanath, S. Collins, D. Mohler, S. Piemonte, S. Prelovsek, A. Schäfer, and S. Weishaeupl, Identifying spin and parity of charmonia in flight with lattice QCD, Phys. Rev. D **99**, 014513 (2019).

[73] S. Chen, C. Shi, Y. Chen, M. Gong, Z. Liu, W. Sun, and R. Zhang, $T_{cc}^{+}(3875)$ relevant DD^{*} scattering from $N_f = 2$ lattice QCD, Phys. Lett. B **833**, 137391 (2022).

[74] C. Morningstar, J. Bulava, B. Singha, R. Brett, J. Fallica, A. Hanlon, and B. Hörz, Estimating the two-particle K-matrix for multiple partial waves and decay channels from finite-volume energies, Nucl. Phys. **B924**, 477 (2017).

[75] A. Abdel-Rehim, C. Alexandrou, J. Berlin, M. Dalla Brida, J. Finkenrath, and M. Wagner, Investigating efficient methods for computing four-quark correlation functions, Comput. Phys. Commun. **220**, 97 (2017).

[76] M. Peardon, J. Bulava, J. Foley, C. Morningstar, J. Dudek, R. G. Edwards, B. Joo, H.-W. Lin, D. G. Richards, and K. J. Juge (Hadron Spectrum Collaboration), A novel quark-field creation operator construction for hadronic physics in lattice QCD, Phys. Rev. D **80**, 054506 (2009).

[77] C. Alexandrou, J. Finkenrath, T. Leontiou, S. Meinel, M. Pflaumer, and M. Wagner, Shallow bound states and hints for broad resonances with quark content $b\bar{c}ud$ in $B - \bar{D}$ and $B^{*} - \bar{D}$ Scattering from lattice QCD, Phys. Rev. Lett. **132**, 151902 (2024).

[78] A. Radhakrishnan, M. Padmanath, and N. Mathur, Study of isoscalar scalar $bc\bar{u}\bar{d}$ tetraquark T_{bc} from lattice QCD, arXiv:2404.08109.